MULTIPLE RESONANCE-ENHANCED 4-WAVE-MIXING PROCESSES IN I-2

Aben, I.; Ubachs, W.M.G.; Levelt, P.; van der Zwan, G.; Hogervorst, W.

published in
Physical Review A. Atomic, Molecular and Optical Physics
1991

DOI (link to publisher)
10.1103/PhysRevA.44.5881

document version
Publisher's PDF, also known as Version of record

Multiple resonance-enhanced four-wave-mixing processes in I_2

Ilse Aben, Wim Ubachs, Pieternel Levelt, Gert van der Zwan, and Wim Hogervorst
Laser Centre Free University Amsterdam, De Boelelaan 1081, 1081 HV Amsterdam, The Netherlands
(Received 14 February 1991; revised manuscript received 24 April 1991)

Resonance-enhanced four-wave-mixing processes were studied in molecular iodine by detection of a wave generated at frequency $\omega_3=2\omega_1-\omega_2$ for a wide range of Raman frequencies $(\omega_1-\omega_2)$. On the basis of known spectroscopic constants of the two electronic states involved, the electronic ground state $X\,^1\Sigma_g^+$ and the electronic excited state $B\,^3\Pi_{u0}^+$, an interpretation of the spectral features in terms of three essentially different four-wave-mixing processes is given. Resonance enhancement through bound states with discrete energy levels and the enhancement effect by dissociative continuum states are considered. In addition to resonance-enhanced coherent anti-Stokes Raman-scattering (CARS) processes, in which the Raman resonances are in the electronic ground state, two resonant schemes are identified in I_2, in which Raman resonances in an excited state are probed: excited-state parametric and nonparametric CARS. The latter process is an example of electronic population transfer in a four-wave-mixing cycle.

PACS number(s): 42.65.Dr, 33.80.−b

I. INTRODUCTION

The I_2 molecule has been the subject of several Raman spectroscopic investigations, using incoherent as well as coherent light-scattering processes. Transitions from the $X\,^1\Sigma_g^+$ electronic ground state to the $B\,^3\Pi_{u0}^+$ excited state [1] or to the low-lying $^1\Pi_{1u}$ repulsive state allow for Raman studies with the excitation frequency tuned to resonance with either discrete energy levels or to a continuum. Rousseau and Williams [2] explained the difference between continuum Raman scattering in I_2, which exhibits resonance enhancement on all rotational transitions, and discrete resonance scattering, which shows distinct spectral lines. In coherent nonlinear Raman-scattering processes the latter features are reproduced, although here the situation is more complicated because of the possibility of multiple resonance enhancement through the many energy levels of the medium.

The theory of four-wave mixing (FWM), of which coherent anti-Stokes Raman scattering (CARS) is a special case, is in an advanced stage of development. A general formula for the third-order nonlinear susceptibility of a medium $\chi^{(3)}$, which governs FWM processes, was derived by Bloembergen, Lotem, and Lynch [3] and Druet *et al.* [4] by application of the density-matrix formalism, calculating the polarization of a medium up to third order. It was shown by Yee *et al.* [5] and later by Prior [6], that all 48 terms of $\chi^{(3)}$ (in the case of three different incident waves) can be derived from a Feynman-type diagrammatic approach. The case of resonance enhancement in CARS and other nonlinear processes was investigated in general by Druet and Taran [7]. Even the subtle effects of Doppler broadening and the possibility of Doppler-free (schemes in) resonance CARS were described in detail [8], although not experimentally demonstrated.

Multiresonant FWM processes were also studied theoretically by Oudar and Shen [9] and later by Mukamel and Loring [10]. For various cases explicit expressions for the resonant nonlinear susceptibilities were derived. In both these theoretical studies, as in the study by Druet and Taran [7], an energy-level scheme of the medium was assumed with only two bound electronic state rovibrational manifolds involved. Ground-state as well as excited-state CARS arising from different terms in the general $\chi^{(3)}$ expression were identified. The specific case of Raman resonance in an excited state corresponds to the process described and measured in Na by Bloembergen and co-workers [3,11].

In the theoretical part of the present study a framework based upon the extra assumption of the existence of a continuum above the two bound electronic states at the two-photon level is proposed. This general energy-level scheme with a bound electronic ground state, a bound excited electronic state one photon above the ground state, and a third continuum state at the two-photon energy level is appropriate in the case of the I_2 molecule. Starting from the 24-term expression for $\chi^{(3)}$ in the case of $\omega_3=2\omega_1-\omega_2$ and retrieving only those terms corresponding to double and triple resonances, ground- and excited-state CARS processes are predicted. One Raman overtone sequence in the electronic ground state and two in the excited state involving resonance enhancement by a continuum are expected from the theory. The Raman resonances in the excited states are enhanced through the continuum at the two-photon level.

Experimentally, three different types of electronic enhancement of CARS signals in molecular iodine have been previously investigated. Beckman *et al.* [12] studied the case of double electronic enhancement by the combined continuum of the $B\,^3\Pi_{u0}^+$ and $^1\Pi_{1u}$ states. Their spectra of continuum-enhanced resonance CARS showed a band structure which is typical in nonresonance CARS; continuum enhancement is nonselective with respect to rotational states. In contrast to nonresonance CARS, however, overtones are strong and the relative intensities are governed by Franck-Condon overlap integrals. Attal, Schnepp, and Taran [13] observed double resonances along with a single example of a triple resonance via discrete energy levels. In the case of such a triple resonance the pump and anti-Stokes frequencies are in resonance with a transition in the $B\,^3\Pi_{u0}^+-X\,^1\Sigma_g^+$ sys-

tem in I_2 along with the Raman resonance in the electronic ground state. Recently Dimov *et al.* [14] in a low-resolution study observed resonance CARS with twofold electronic enhancement: one by a discrete level and one by the continuum part of the $B\,^3\Pi_{u0}^+$ state.

In the experimental part of the present study a variety of multiple resonance FWM features were observed using a two-color setup, with a fixed frequency pump wave ω_1 and a tunable Stokes wave ω_2. Three sequences of repeating groups of spectral lines were recorded in a wide frequency range for a Raman shift $\omega_1-\omega_2=380-2300$ cm^{-1}. All resonances in the FWM spectra are produced by coincidental enhancement of the FWM signal when one or more of the frequencies are in resonance with an optically allowed transition in the medium. Resonances were identified on the basis of an assignment with quantum numbers of the different states involved. The molecular constants of Luc [15] were used to calculate the transitions in the $B\,^3\Pi_{u0}^+-X\,^1\Sigma_g^+$ system in I_2. All specific features observed could be accounted for by the predicted processes.

A first sequence of nearly identical groups of spectral lines could be assigned to Raman resonances in the ground electronic $X\,^1\Sigma_g^+$ state, similar to the observations of Dimov *et al.* [14]. This sequence extended into a region where it showed up as a triply discrete resonance, similar to the one observed by Attal, Schnepp, and Taran [13]. Two other sequences, corresponding to Raman resonances in the excited electronic $B\,^3\Pi_{u0}^+$ state were observed as well; one is a parametric FWM process and the other is a nonparametric FWM process.

II. THEORETICAL FRAMEWORK

A. Resonance enhancement in a generalized molecular energy structure

The elements of a third-order nonlinear susceptibility tensor $\chi_{ijkl}^{(3)}$ determine the intensity of the generated FWM signal at a frequency ω by

$$I_{\mathrm{FWM}}(\omega)\propto\left|\sum_{i,j,k,l}\chi_{ijkl}^{(3)}(\omega)\right|^2, \tag{1}$$

where $ijkl$ are indices of a fourth rank tensor, related to vector orientations of the applied and induced electric fields. Under the specific conditions of an isotropic medium and all fields linearly polarized parallel to a defined z axis only the χ_{zzzz} tensor element remains as an independent parameter. Therefore the tensor indices are dropped in the following. The theoretical as well as experimental implications of arbitrary polarization in resonance CARS will be treated in a forthcoming paper [16].

The $\chi^{(3)}$ element can be derived by third-order perturbation expansion of the polarization induced by the applied electric fields in the medium. For general expressions of $\chi^{(3)}$, including all resonant and nonresonant contributions to the nonlinear third-order susceptibility reference is made to the literature [3,6,7]. In the most general case of a four-wave-mixing process with a wave generated at frequency $\omega=\pm\omega_1\pm\omega_2\pm\omega_3$ by three different frequencies, a 48-term expression for $\chi^{(3)}(\omega)$ results. When the frequency of the generated wave is $\omega_3=2\omega_1-\omega_2$, as in the case of the present study, $\chi^{(3)}(\omega)$ contains only 24 terms.

A nonlinear medium of molecules in the gas phase will now be considered with a generalized energy-level structure as shown in Fig. 1(a). Levels $|0\rangle$ and $|v\rangle$ represent rovibrational states in a bound electronic ground state $|g\rangle$, $|0\rangle$ being the vibrational ground state. Levels $|n\rangle$, $|n'\rangle$, $|n''\rangle$, and $|n'''\rangle$ are rovibrational levels in a bound, electronically excited state $|e\rangle$. $|n'''\rangle$ may also refer to the dissociative continuum of that electronic state in the energy range above its dissociation limit. The states $|m\rangle$ represent virtual states below the initial state $|0\rangle$. The distinction between states $|n\rangle$, $|n'\rangle$, $|n''\rangle$, and $|n'''\rangle$ is made to stress that resonances in different FWM processes may involve vibrational states in a different energy region of the same electronically excited state. This bound excited electronic state is separated from the electronic ground state by the energy of one photon. The level $|c\rangle$ denotes a continuum at the two-photon energy $2\omega_1$. The incorporation of this continuum state $|c\rangle$ has implications which lead to differences with the results obtained by Attal *et al.* [13,7], Oudar and Shen [9], and Mukamel and Loring [10]. They also derived general expressions for resonant four-wave mixing at $\omega_3=2\omega_1-\omega_2$ for the case of $\omega_1>\omega_2$. However, they assumed an energy scheme with two bound electronic states separated in energy by one photon without considering enhancement by a (contiuum) state at the two-photon level. As a consequence excited-state CARS processes were not observed.

Assuming this generalized energy-level structure, and retrieving only those terms leading to the strongest resonance enhancement (double and triple resonances), the number of relevant terms in $\chi^{(3)}(\omega_3)$ reduces to the following eight:

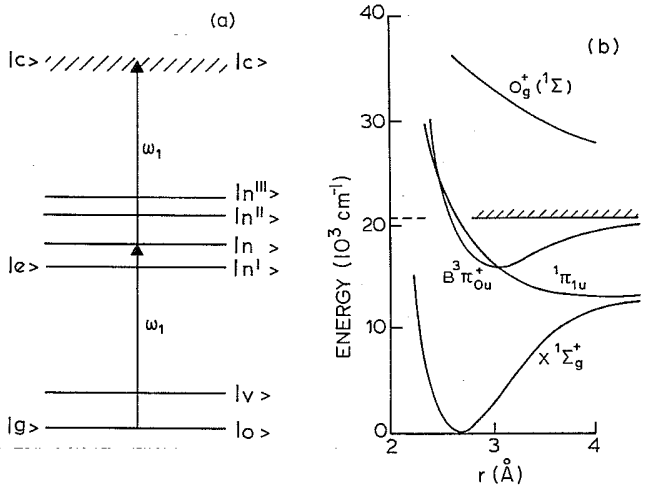

FIG. 1. (a) Energy-level scheme for a generalized molecule. Horizontal solid lines refer to bound states while the shaded area represents a continuum state. $|n'''\rangle$ is either a discrete state or it represents the dissociative continuum above the electronically excited state. (b) Potential curves of I_2. The fixed pump laser frequency ω_1 is in near resonance with the $B\,^3\Pi_{u0}^+-X\,^1\Sigma_g^+$ transitions of the particular rovibrational substates $|n\rangle$ and $|0\rangle$ listed in Table I.

$$\chi^{(3)}_{\mathrm{I}}(\omega_3)\propto N\sum_{0,n,n''',v}\rho^{(0)}_{00}\frac{\mu_{0n'''}\mu_{n'''v}\mu_{vn}\mu_{n0}}{(\omega_{n0}-\omega_1-i\Gamma_{n0})(\omega_{v0}-\omega_1+\omega_2-i\Gamma_{v0})(\omega_{n'''0}-\omega_3-i\Gamma_{n'''0})}\ , \tag{2a}$$

$$\chi^{(3)}_{\mathrm{II}}(\omega_3)\propto N\sum_{0,n,c,n''}\rho^{(0)}_{00}\frac{\mu_{0n''}\mu_{n''c}\mu_{cn}\mu_{n0}}{(\omega_{n0}-\omega_1-i\Gamma_{n0})(\omega_{c0}-2\omega_1-i\Gamma_{c0})(\omega_{n''0}-\omega_3-i\Gamma_{n''0})}\ , \tag{2b}$$

$$\chi^{(3)}_{\mathrm{III(a)}}(\omega_3)\propto N\sum_{0,n,c,n'}\rho^{(0)}_{00}\frac{\mu_{0n'}\mu_{n'c}\mu_{cn}\mu_{n0}}{(\omega_{n0}-\omega_1-i\Gamma_{n0})(\omega_{nn'}-\omega_1+\omega_2-i\Gamma_{nn'})(\omega_{cn'}-\omega_3-i\Gamma_{cn'})}\ , \tag{2c}$$

$$\chi^{(3)}_{\mathrm{III(b)}}(\omega_3)\propto N\sum_{0,n,c,n'}\rho^{(0)}_{00}\frac{\mu_{0n'}\mu_{n'c}\mu_{cn}\mu_{n0}}{(\omega_{n'0}-\omega_2+i\Gamma_{n'0})(\omega_{nn'}-\omega_1+\omega_2-i\Gamma_{nn'})(\omega_{cn'}-\omega_3-i\Gamma_{cn'})}\ , \tag{2d}$$

$$\chi^{(3)}_{\mathrm{III(c)}}(\omega_3)\propto N\sum_{0,n,c,n'}\rho^{(0)}_{00}\frac{\mu_{0n'}\mu_{n'c}\mu_{cn}\mu_{n0}}{(\omega_{n0}-\omega_1-i\Gamma_{n0})(\omega_{c0}-2\omega_1-i\Gamma_{c0})(\omega_{cn'}-\omega_3-i\Gamma_{cn'})}\ , \tag{2e}$$

$$\chi^{(3)}_{\mathrm{IV(a)}}(\omega_3)\propto N\sum_{0,n,n',m}\rho^{(0)}_{00}\frac{\mu_{0n'}\mu_{n'm}\mu_{mn}\mu_{n0}}{(\omega_{n0}-\omega_1-i\Gamma_{n0})(\omega_{nn'}-\omega_1+\omega_2-i\Gamma_{nn'})(\omega_{nm}-\omega_3-i\Gamma_{nm})}\ , \tag{2f}$$

$$\chi^{(3)}_{\mathrm{IV(b)}}(\omega_3)\propto N\sum_{0,n,n',m}\rho^{(0)}_{00}\frac{\mu_{0n'}\mu_{n'm}\mu_{mn}\mu_{n0}}{(\omega_{n'0}-\omega_2+i\Gamma_{n'0})(\omega_{nn'}-\omega_1+\omega_2-i\Gamma_{nn'})(\omega_{nm}-\omega_3-i\Gamma_{nm})}\ , \tag{2g}$$

$$\chi^{(3)}_{\mathrm{IV(c)}}(\omega_3)\propto N\sum_{0,n,n',m}\rho^{(0)}_{00}\frac{\mu_{0n'}\mu_{n'm}\mu_{mn}\mu_{n0}}{(\omega_{n'0}-\omega_2+i\Gamma_{n'0})(\omega_{0m}-\omega_1+\omega_2-i\Gamma_{0m})(\omega_{nm}-\omega_3-i\Gamma_{nm})}\ . \tag{2h}$$

In these equations a one-photon electronic dipole transition from state $|j\rangle$ to state $|i\rangle$ has a frequency ω_{ij} and a transition moment $\mu_{ij}=\langle i|\mu|j\rangle$. The fractional initial population of state $|i\rangle$ is given by $\rho^{(0)}_{ii}$ and N is the total density of the molecules. In the derivation of Eq. (2) only contributions to $\chi^{(3)}$ with a nonzero $\rho^{(0)}_{00}$ have been retained. Furthermore, terms with antiresonant denominators, usually lumped together in a nonresonant term $\chi^{(3)}_{NR}$, are automatically dropped in the procedure followed here.

Resonance enhancement of the FWM signal is accomplished when one (or more) of the energy differences in the denominator vanishes. Such a resonance enhancement is damped by the relaxation parameters Γ_{ij} [17,9] phenomenologically introduced by Bloembergen [3]:

$$\Gamma_{ij}=\tfrac{1}{2}(\Gamma_{ii}+\Gamma_{jj})+\Gamma^{p}\ . \tag{3}$$

Γ_{ii} and Γ_{jj} for the present case of free molecules are related to the radiative lifetimes of levels $|i\rangle$ and $|j\rangle$ (including the effect of inelastic or quenching collisions), and Γ^{p} is the collisional dephasing rate related to elastic collisions. The denominators in Eq. (2) determine the frequency combinations ω_1,ω_2 and $\omega_3=2\omega_1-\omega_2$ for which enhancement in FWM signal can be achieved. When the frequencies are tuned into exact resonance with an allowed transition (ω_{ij}), the relaxation parameter Γ_{ij} will predominantly determine the overall enhancement of a particular process. In resonances produced by coherences between bound states, the collisional damping will determine the relaxation and therefore the enhancement. In resonances involving a dissociative continuum state the short lifetime of the continuum state determines Γ_{ij}. In the latter case the resonance enhancement will therefore be weaker. Similarly, a detuning from resonance represented by a frequency offset $\delta\omega_{ij}=\omega-\omega_{ij}$ will influence the value of $\chi^{(3)}$. Relaxation damping parameters Γ_{ij} and detuning parameter $\delta\omega_{ij}$ are thus equivalent in their quantitative effect upon resonance enhancement in FWM.

The third-order nonlinear susceptibility representing all different possible double and triple resonance features with $\omega_3=2\omega_1-\omega_2$ is equal to the sum of the eight terms given in Eq. (2). In principle the intensity of FWM signals determined by the absolute square of the total third-order nonlinear susceptibility [Eq. (1)] therefore also includes interferences between different terms. In multiresonance FWM, however, distinct spectral lines appear at particular frequency pairs (ω_1,ω_2), and here a specific term dominates the total $\chi^{(3)}$. Contributions of processes at different frequencies ω_3 will therefore be treated separately and the interference effect neglected.

The expressions in Eq. (2) can be visualized in two different ways, one using double-Feynman diagrams (Fig. 2) and the other energy diagrams (Fig. 3). The advantage of the double-Feynman diagrams is that there is a one-to-one correspondence between each specific term in $\chi^{(3)}$ and a particular double-Feynman diagram. Furthermore, the double-Feynman diagrams represent all different *time-ordering* combinations of the three interacting waves. The three double-Feynman diagrams IIIa–IIIc in Fig. 2 differ only in the time ordering of the interacting waves. The same holds for IVa–IVc. Terms of $\chi^{(3)}$ can be derived in mathematical form from the double-Feynman diagrams in a straightforward manner by using the substitution rules given by different authors [6,5,18]. The algebraic expression corresponding with each Feynman diagram can be evaluated without calculating lower-order processes, as required in the perturbative derivation of $\chi^{(3)}$. In fact the eight relevant terms of $\chi^{(3)}$ given in Eq. (2) were derived independently by first considering possible resonances in an energy diagram, followed by construction of all possible time-ordered Feynman diagrams with translation into a mathematical for-

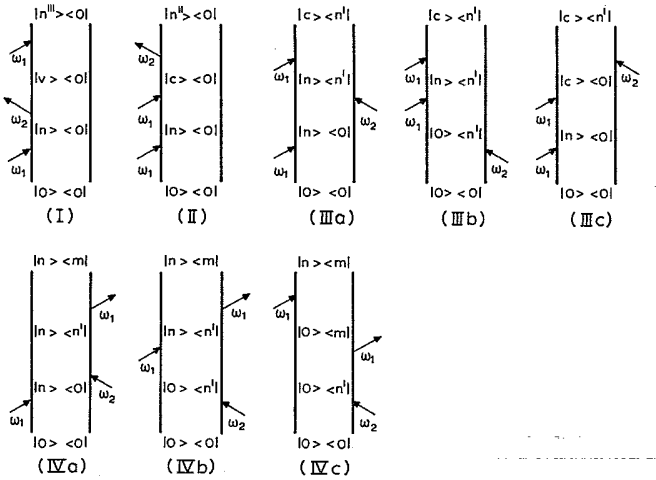

FIG. 2. Double-Feynman diagrams representing possible multiresonance FWM schemes, fitting in the generalized energy-level scheme shown in Fig. 1. The convention of Nibler and Yang [31] is followed in order to omit the interaction of the fourth photon generated as this is of no importance for the translation of Feynman diagrams into mathematical expressions for terms in $\chi^{(3)}$. Note that the diagrams III(a), III(b), and III(c) differ only in the time ordering of the interactions. The same is true for the diagrams of scheme IV. There is a one-to-one relation between the Feynman diagrams I–IV and the terms of $\chi^{(3)}$ given in Eq. (2) with the same subscripts. The labeling of the states $|0\rangle$, $|v\rangle$, $|n\rangle$, etc. is according to that used in Eq. (2).

mula. When the interaction vertices in the double-Feynman diagrams occur on one side only (e.g., in Fig. 2, I and II) the processes are called parametric [7], whereas those with the vertices on both sides (in Fig. 2, III and IV) are called nonparametric. In the case of a multicolor FWM process this implies that the initial and final states are identical in parametric and different in nonparametric processes.

An advantage of the use of the energy diagrams is that the resonances between incident waves and transitions in the medium in a FWM process are clearly visualized. The use of energy-level diagrams has, however, some disadvantages. It should be realized that these diagrams are merely used to indicate the resonances in the different processes, and may not be viewed as representing a time-ordered sequence of one-photon absorptions or emissions. Furthermore, no one-to-one correspondence between the energy diagrams and the terms of $\chi^{(3)}$ exists as in the case of the double-Feynman diagrams. The processes of Figs. 3(a)–3(e) all correspond to the term $\chi_{\mathrm{I}}^{(3)}$, of Fig. 3(f) to the term $\chi_{\mathrm{II}}^{(3)}$, of Fig. 3(g) to $\chi_{\mathrm{III}}^{(3)}$, and of Fig. 3(h) to $\chi_{\mathrm{IV}}^{(3)}$, respectively.

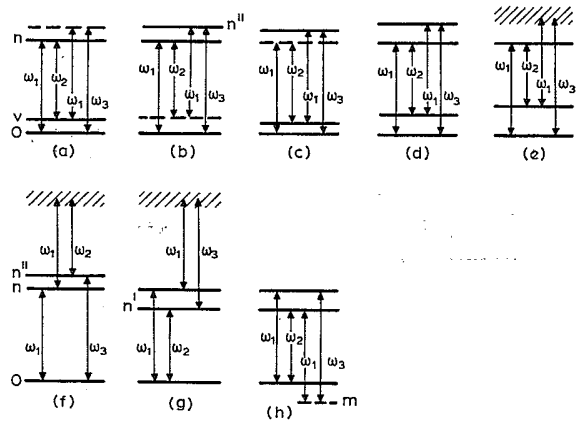

FIG. 3. The energy diagrams and resonances of FWM processes $\omega_3=2\omega_1-\omega_2$. Dashed lines represent virtual states, whereas the shaded area refers to a continuum. Again, labeling of the states is consistent with that used in Eq. (2).

In the following the expected spectral positions of the FWM resonances, connected with the eight terms of $\chi^{(3)}$ in Eq. (2), and related energy diagrams of Fig. 3 will be discussed for the condition that ω_1 is fixed and ω_2 is variable.

All possible double and triple resonances denoted by $\chi_{\mathrm{I}}^{(3)}$ are represented by the processes in Figs. 3(a)–3(e), and are commonly referred to as resonance-enhanced coherent anti-Stokes Raman processes. The processes shown in Figs. 3(a)–3(c) are called laser-enhanced Raman, double-electronic, and anti-Stokes-enhanced Raman resonances, respectively. In these processes two discrete resonances and one detuning from resonance are involved. These twofold resonance processes have been described in detail by Attal *et al.* in various papers [13,7] and are not discussed here. In the limit of detuning approaching zero these three processes are identical. This is the triply discrete resonance-enhanced FWM process of Fig. 3(d), where the product of resonance denominators in $\chi_{\mathrm{I}}^{(3)}$ is equal to $\Gamma_{n0}\Gamma_{v0}\Gamma_{n'''0}$. Because all four states involved ($|0\rangle$, $|n\rangle$, $|v\rangle$, and $|n'''\rangle$) are discrete energy levels, $\chi^{(3)}$ is highly enhanced.

When the anti-Stokes (ω_3) resonance is a continuum resonance, the process of energy diagram Fig. 3(e) relates to $\chi_{\mathrm{I}}^{(3)}$. This FWM process has been observed by Dimov *et al.*[14]. As ω_2 is tuned in Raman resonances ($\omega_1-\omega_2=\omega_{v0}$) in the electronic ground state are probed and overtones will be observed in the FWM spectrum. This is similar to the appearance of overtones in spontaneous resonance Raman processes. For this process the first frequency factor in the denominator of $\chi_{\mathrm{I}}^{(3)}$ is assumed to be resonant and therefore introduces a selectivity for states $|0\rangle$ and $|n\rangle$ through $\omega_1\approx\omega_{n0}$. As the pump frequency ω_1 is kept fixed during the experiment, the ω_1 resonance acts as a constant "state selector" for the overall FWM process.

The resonances in $\chi_{\mathrm{II}}^{(3)}$ correspond to those shown in the energy diagram of Fig. 3(f). Again the resonance $\omega_1\approx\omega_{n0}$ acts as a state selector for the overall FWM process. Tuning ω_2 will now give Raman overtones in the excited electronic state as the resonances $\omega_3=\omega_{n''0}$ and $\omega_1\approx\omega_{n0}$ correspond to $\omega_3-\omega_1=\omega_{n''n}$. As $\omega_3>\omega_1$, the states $|n''\rangle$ are higher in energy than the states $|n\rangle$ selected through the ω_1 resonance.

The double resonances of Fig. 3(b) appear at the same frequency positions ($\omega_1-\omega_2$) as in the process described by $\chi_{\mathrm{II}}^{(3)}$. In both processes the first and last factor in the denominator of the corresponding terms in Eq. (2) are

on-resonance and identical. The other factor in the denominator is either off-resonant [in case 3(b)] or involves a continuum resonance [in case 3(f)], and so does not introduce an extra selectivity to the overall FWM process. Both processes thus contribute to the same lines in the spectrum. In $\chi^{(3)}_{II}$ the resonance enhancement on $2\omega_1=\omega_{c0}$ is damped by a continuum relaxation parameter Γ_{c0}, whereas the enhancement in $\chi^{(3)}_{I}$ is limited by the detuning $\delta\omega=(\omega_1-\omega_2)-\omega_{v0}$.

The terms $\chi^{(3)}_{III,a,b,c}$ in Eq. (2) correspond to the three different time-ordered double-Feynman diagrams IIIa–IIIc of Fig. 2 and also with the resonances shown in the single energy diagram of Fig. 3(g). These terms have the same discrete resonances so they will contribute to the same lines in the FWM spectrum. However, $\chi^{(3)}_{III(c)}$ contains two factors in the denominator of Eq. (2e) with large continuum relaxation parameters Γ_{ci}. The contribution of $\chi^{(3)}_{III(c)}$ is smaller than that of $\chi^{(3)}_{III(a)}$ and $\chi^{(3)}_{III(b)}$, which only have a single continuum relaxation parameter damping the resonance enhancement. Therefore, $\chi^{(3)}_{III(c)}$ will be ignored in the following. The ω_1 resonance again serves as a state selector, which is obvious in $\chi^{(3)}_{III(a)}$. In $\chi^{(3)}_{III(b)}$ the two resonant factors $\omega_2=\omega_{n'0}$ and $\omega_1-\omega_2=\omega_{nn'}$ combine to $\omega_1=\omega_{n0}$. Raman resonances $\omega_1-\omega_2=\omega_{nn'}$ in the excited electronic state at the one-photon level are probed by tuning ω_2. In this case state $|n'\rangle$ has a lower energy than $|n\rangle$ because $\omega_1>\omega_2$.

In Fig. 3(h) the resonances in the $\chi^{(3)}_{IV}$ terms are shown. The energy-level diagram indicates that, similar to the $\chi^{(3)}_{III}$ terms represented in Fig. 3(g), the selectivity in the FWM spectra is given by a Raman resonance between electronically excited states $|n'\rangle$ and $|n\rangle$. Again ω_1 is a state selector for rotational states, and the terms in $\chi^{(3)}_{III}$ and $\chi^{(3)}_{IV}$ contribute to the same lines in the FWM spectra. The continuum resonance at $|c\rangle$ in Fig. 3(g) is replaced by a detuning in Fig. 3(h) which is about equal to the frequency separation between both waves, $\delta\omega_{det}=\omega_1-\omega_2$. Inspection of the mathematical expressions of Eq. (2), yields the same result. The enhancement of $\chi^{(3)}$ is proportional to $(\Gamma_{n0}\Gamma_{nn'}\Gamma_{cn'})^{-1}$ and $(\Gamma_{n'0}\Gamma_{nn'}\Gamma_{cn'})^{-1}$ for $\chi^{(3)}_{III(a)}$ and $\chi^{(3)}_{III(b)}$, respectively. For the terms $\chi^{(3)}_{IV(a)}$ and $\chi^{(3)}_{IV(b)}$ the enhancement proportionality factors are $(\Gamma_{n0}\Gamma_{nn'}\delta\omega_{det})^{-1}$ and $(\Gamma_{n'0}\Gamma_{nn'}\delta\omega_{det})^{-1}$. The term $\chi^{(3)}_{IV(c)}$ is, similarly to $\chi^{(3)}_{III(c)}$, left out of the discussion. The FWM enhancement by this term is very small because the detuning $\delta\omega_{det}=\omega_1-\omega_2$ appears twice in the denominator. The relative intensity enhancements by $\chi^{(3)}_{III}$ [scheme (g)] and $\chi^{(3)}_{IV}$ [scheme (h)], which contribute to the same spectral features, can be determined from a comparison of the relaxation damping by a continuum $\Gamma_{cn'}$ and the detuning $\delta\omega_{det}=\omega_1-\omega_2$. In overtone vibrational CARS the frequency separation $\omega_1-\omega_2$ is generally larger than 500 cm^{-1}. This holds at least for the present study. The relaxation damping $\Gamma_{cn'}$ is related to the time scale of dissociation in a repulsive continuum state $|c\rangle$. Although not applicable to all examples of molecular dissociation, a time scale ranging from 0.1 to 10 ps will cover most cases. This corresponds to damping parameters between 0.5 and 50 cm^{-1}. Based upon these estimates the contributions of terms $\chi^{(3)}_{IV}$ are expected to be smaller than those of $\chi^{(3)}_{III}$. The appropriate Franck-Condon overlap and electronic transition moments should also be taken into account. These are not known for transitions to this continuum.

To summarize, it has been shown that essentially three sequences of coherent Raman resonances are to be expected: one Raman overtone sequence in the electronic ground state and two Raman overtone series in the electronically excited state.

B. Characteristics of I_2 as a medium for FWM

In Sec. II A four-wave-mixing processes were analyzed by inspection of all terms in $\chi^{(3)}$ that give rise to (at least twofold) resonance enhancement in a molecular medium with a generalized energy-level structure as shown in Fig. 1(a). The results obtained thusfar are applicable to any medium with a similar quantum structure. Now the specifics of the molecular structure of I_2 and some characteristics of molecular spectroscopy relevant for the present work will be introduced.

The potential curves for I_2 are shown in Fig. 1(b). The electronic ground state $X\,^1\Sigma_g^+$ and the bound electronically excited state $B\,^3\Pi_{u0}^+$, separated in energy by a visible photon, are accurately characterized in the work of Luc [15]. Both electronic states $X\,^1\Sigma_g^+$ and $B\,^3\Pi_{u0}^+$ have $\Omega=0$, so the $\Delta J=\pm1$ selection rule holds for the one-photon transition [19]. In the literature there has been some dispute on the existence of a gerade bound state in I_2 at an energy of about 35 000 cm^{-1}. In several reports on one-color multiphoton ionization (MPI) [20,21] and third-harmonic generation [22], the existence of such a stable electronic state is claimed. Tai, Dalby, and Giles [22] recorded a third-harmonic four-wave-mixing spectrum in the one-photon region 17 900–18 600 cm^{-1} and postulated resonance enhancement at the one-photon ($B\,^3\Pi_{u0}^+$ state) and the two-photon level. They calculated molecular constants for a 0_g^+ state in the two-photon energy region and obtained a vibrational interval of 133 cm^{-1}. Brand and Hoy [23], however, successfully reassigned the FWM spectrum of Tai, Dalby, and Giles assuming resonance enhancement of the one- and three-photon levels. Lehmann, Smolarek, and Goodman [20] interpreted a MPI spectrum as due to a stable state of 0_g symmetry at $T_e=35\,869$ cm^{-1} with $\omega_e=104$ cm^{-1}, assuming this level to be excited by two-photon absorption via the $B\,^3\Pi_{u0}^+$ state. More recently King and McLean [24] reported one- and two-color absorption spectra of iodine in the same region as Lehmann, Smolarek, and Goodman. However, they found no evidence for stable excited states near 35 000 cm^{-1}. Furthermore, Sander and Wilson [25,26] performed double absorption photofragment spectroscopy on I_2 at 532 nm and found evidence for a dissociative $0_g^+(^1\Sigma)$ state at approximately 37 700 cm^{-1}. This was confirmed by Kasatani *et al.* [27] in a three-photon absorption experiment via the bound $B\,^3\Pi_{u0}^+$ state and the repulsive 0_g^+ state ($\Omega=0$). Based upon the existing spectroscopic knowledge of the I_2 molecule the assumption of a continuum at the $2\omega_1$ frequency above the ground state seems to be justified.

In the one-photon energy range a repulsive $^1\Pi_{1u}$ state

exists [see Fig. 1(b)] in addition to the bound $B\,^3\Pi_{u0}^+$ state. A study of resonance (spontaneous) Raman spectroscopy in I_2 by Kiefer and Baierl [28] showed that in the energy range from the B-state dissociation limit (20 043.063±0.020 cm^{-1} [29]) up to 3000 cm^{-1} above this limit, the contribution of this repulsive $^1\Pi_{1u}$ state to the resonance enhancement is small compared to the contribution of the dissociative continuum connected to the $B\,^3\Pi_{u0}^+$ state itself.

It may be concluded that the generalized energy-level structure of Fig. 1(a) is appropriate to represent the real quantum structure of the I_2 molecule. The $X\,^1\Sigma_g^+$ state is the bound electronic ground state $|g\rangle$. The $B\,^3\Pi_{u0}^+$ state is the electronically excited bound state at the one-photon level $|e\rangle$, and the $0_g^+(^1\Sigma)$ repulsive state is the continuum $|c\rangle$ at the two-photon level.

III. EXPERIMENT

In a standard colinear CARS setup a Quanta Ray DCR3: Nd:YAG (neodymium-doped yttrium aluminum garnet) laser operating at 10 Hz was used in combination with a dye laser. The second harmonic of the injection-seeded Nd:YAG laser (estimated bandwidth 0.005 cm^{-1} at 532 nm) acted as the pump beam (ω_1) in the FWM process and synchronously pumped a Quanta Ray PDL2 tunable dye laser, generating the Stokes frequency (ω_2) with a linewidth of about 0.3 cm^{-1}. Laser powers in the interaction region were about 10 mJ per pulse (in 7 ns) for the pump beam and typically 4 mJ (in 5 ns) for the Stokes beam. A spectral region of 380–2300 cm^{-1} for the Raman shift $\omega_1-\omega_2$ was covered using the dyes fluorescein-27 and rhodamine 590, 610, and 640 as well as DCM. Temporal overlap of the two laser pulses was carefully checked. The polarizations of the laser beams were chosen to be linear and parallel during all experiments.

The two beams were spatially overlapped using a dichroic mirror and focused into the I_2 cell with a 25-cm focal length lens. The cell length used in these experiments was 40 cm, and spectra were obtained in pure iodine at the saturated room-temperature vapor pressure of 0.3 torr. The generated FWM signal at the anti-Stokes frequency $\omega_3=2\omega_1-\omega_2$ was separated from the pump and Stokes beam using interference filters. They were then focused onto a 0.6-m triple monochromator (SPEX) set at ω_3. In order to suppress nonresonant CARS signals from air, the dichroic mirror and the interference filter were mounted as close as possible to the iodine cell. The ω_3 beam was detected with a photomultiplier and the signal digitized and stored on a VME computer via a Stanford Research Systems boxcar integrator (SR-250) and interface (SR-245). By scanning a narrow transmission window of the monochromator around the frequency ω_3, it was verified that the blue light was indeed generated by a coherent FWM process, and not by a two-color induced fluorescence process. In the latter case a band system around ω_3 is to be expected. The time profile of the generated signal was also found to be consistent with a FWM process. The spectra were obtained by averaging ten laser shots per frequency setting.

The linearity of the scan was monitored by simultaneously recording the transmission fringes of a Fabry-Pérot etalon (FSR=2.45 cm^{-1}). The étalon markers also allowed for an accurate determination (within 0.1 cm^{-1}) of the relative frequency separations between adjacent spectral lines and the linewidths of the FWM resonances.

Absolute wavelengths were measured with an accuracy of 0.2 cm^{-1} by means of a home-built echelle-grating wavelength meter. The fixed frequency ω_1 of the narrow-band pump beam was 18 788.3±0.2 cm^{-1}.

IV. OBSERVATION AND INTERPRETATION OF SPECTRAL FEATURES

The FWM spectra of I_2 recorded in the wavelength region under investigation showed three different series of repetitive groups of narrow spectral lines with different frequency separations. These separations correspond to different vibrational spacings in the electronic states $X\,^1\Sigma_g^+$ and $B\,^3\Pi_{u0}^+$, indicating the appearance of Raman overtones. The separations in one of these series decrease with increasing ω_2 whereas in the other series they increase. The anharmonicity of the $X\,^1\Sigma_g^+$ and $B\,^3\Pi_{u0}^+$ potential curves suggests that continuously higher excited vibrational levels are probed in the former case, and continuously lower vibrational levels in the latter case. One of the series with a repetitive frequency separation of about 200 cm^{-1}, related to the $X\,^1\Sigma_g^+$ ground-state vibrational splitting, extends into a region (at $\omega_1-\omega_2<1200$ cm^{-1}) where a few lines within each group are an order of magnitude stronger than all other observed features.

An accurate analysis of the observed FWM spectra was possible using known molecular constants of the electronic states $X\,^1\Sigma_g^+$ and $B\,^3\Pi_{u0}^+$. The energies of the rovibrational levels in $X\,^1\Sigma_g^+$ and $B\,^3\Pi_{u0}^+$ were determined by Luc *et al.* [15] to an accuracy of 0.0015 cm^{-1}. The study of multiresonant FWM in I_2 thus has the advantage that the resonant character of each wave in the energy-level structure can be identified spectroscopically. Different four-wave-mixing schemes, shown in Fig. 3 were required to account for all the features in the spectra. Attention will be focused on the processes that give rise to the Raman resonances in the electronic ground state $X\,^1\Sigma_g^+$ [schemes (d) and (e) of Fig. 3], as well as in the electronic excited state $B\,^3\Pi_{u0}^+$ [schemes (f) and (g)].

As discussed in Sec. II, a FWM process is equivalent to a time-ordered sequence of four interactions. Because the spectroscopic notation developed by Druet and Taran [7] was found to be not fully suited for an unambiguous description of the different FWM processes presently observed, a new notation is introduced. The discrete, (nearly) resonant interactions are considered to be one-photon P or R transitions since $\Delta J=0$ is forbidden (in the case of $B\,^3\Pi_{u0}^+-X\,^1\Sigma_g^+$ transitions). Continuum resonances or resonances involving a large detuning are represented by two-photon interactions ^2O, ^2Q, or ^2S as in Raman spectroscopy. The time-ordered transition sequence indicated in the double-Feynman diagrams of Fig. 2 is maintained in the notation. In the nonparametric process represented by the Feynman diagrams III the time sequence of III(b) was adopted. As an example $[P,^2Q,R]53$ represents an excited-state parametric CARS process

starting at the $X\,^1\Sigma_g^+$, $v''=0$, $J''=53$ level. One-photon absorption in a P transition is followed by a continuum-enhanced Raman Q transition and an emission in an R transition. Wherever necessary the vibrational levels are specified with the resonant transitions as well. In the parametric processes $\Delta J=0$ holds for the full cycle of four-photon interactions because of energy conservation. In the nonparametric process the rotational quantum number J for the initial state $|0\rangle$ and final state differ by 1.

Selectivity is introduced in all these processes by near absorption resonances of ω_1. Figure 4 shows the absorption spectrum of I_2 near the fixed frequency of the pump beam at $\omega_1=18\,788.3(2)$ cm^{-1}, reproduced from the atlas of Gerstenkorn and Luc [1]. The absolute frequency of the injection-seeded frequency-doubled Nd: YAG laser is measured within 0.2 cm^{-1}, but its actual bandwidth is extremely narrow (<0.005 cm^{-1}). The assignment in Fig. 4 is deduced from a calculation using the molecular constants of Luc [15]. FWM processes involving transitions with a frequency close to ω_1 will be most strongly enhanced, since then $\omega_1\approx\omega_{n0}$ [Eq. (2)]. The I_2 $B\,^3\Pi_{u0}^+$–$X\,^1\Sigma_g^+$ absorption lines closest to the pump frequency are given in Table I, with calculated transition frequencies, detunings $\delta\omega=\omega_1-\omega_{n0}$ from the resonance frequency, and fractional population density of the rovibrational starting level involved. Here the influence of nuclear spin statistics, giving rise to higher populations in the odd-J states, is accounted for. All pronounced spectral features observed are related to these $P(53)$, $R(56)$, $P(83)$, and $P(103)$ transitions, and the fixed frequency ω_1 therefore acts as a "J-state selector." It should be noted that on a particular FWM resonance the entire signal is produced by the small fraction of molecules in one initial state only. In FWM the intensities are proportional to the square of the density of particles in the ground state $[N\rho_{00}^{(0)}]^2$ whereas in linear absorption (Fig. 4) they are proportional to $N\rho_{00}^{(0)}$. As a consequence only FWM signals involving the $X\,^1\Sigma_g^+, v''=0$ ground state need to be considered, represented by $|0\rangle$ as in the expression of Eq. (2).

In the following subsections the spectral features of the different FWM processes denoted by the energy-level diagrams of Figs. 3(d)–3(g) will be discussed.

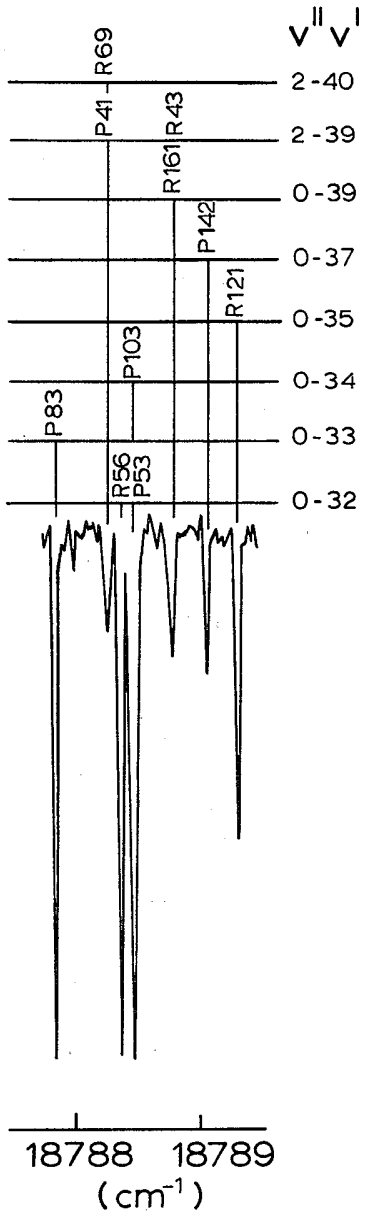

FIG. 4. Absorption spectrum of I_2 $B\,^3\Pi_{u0}^+$–$X\,^1\Sigma_g^+$ close to the ω_1 pump laser frequency, reproduced from [1]. The calculated assignment is based upon the molecular constants of [15].

TABLE I. Absorption lines in the $B\,^3\Pi_{u0}^+$–$X\,^1\Sigma_g^+(v',v'')$ band system in near resonance with the frequency of the narrow-band pump beam (18 788.3 cm^{-1}). Also listed is the detuning for each transition from resonance (in cm^{-1}) and the relative population of the ground states. The accuracy in the offset is determined by the wavelength meter (0.2 cm^{-1}).

Absorption line	Frequency[a]	Offset $\delta\omega=\omega_1-\omega_{v0}$	Relative population (%)
$P(53)(32,0)$	18 788.45	−0.2	0.84
$R(56)(32,0)$	18 788.34	−0.0	0.60
$P(83)(33,0)$	18 787.81	+0.5	0.64
$P(103)(34,0)$	18 788.44	−0.1	0.41

[a]Calculated from spectroscopic constants of Luc [15].

A. Resonance-enhanced ground-state CARS

An example of the observed spectra of the Raman overtone resonances $\Delta v=6$ and 8 is shown in Fig. 5. The notation Δv identifies a Raman resonance $\omega_1-\omega_2=\omega_{v0}$ in the electronic ground state $X\,^1\Sigma_g^+$ between states $|0\rangle$ and $|v\rangle$. All of the spectra are similar in appearance in this Raman overtone sequence, which was observed up to $\Delta v=13$ in the frequency range $\omega_1-\omega_2=1200$–2300 cm^{-1}. Discrete resonance enhancement is achieved in two factors in the denominator of $\chi_I^{(3)}$, $\omega_1\approx\omega_{n0}$ and $\omega_1-\omega_2=\omega_{v0}$. Continuum resonance enhancement occurs for the anti-Stokes interaction represented by the third factor in the denominator of $\chi_I^{(3)}$. This is the process corresponding to scheme (e) in Fig. 3. The discrete resonance (with small detuning $\delta\omega=\omega_1-\omega_{n0}$) on the fixed frequency ω_1 acts as a J-state selector and for the states thus selected (Table I) a second resonance Raman condition ($\omega_1-\omega_2=\omega_{v0}$) can be fulfilled by tuning ω_2. The combination of two interactions, in the time ordering of diagram I in Fig. 2, then determines the frequency positions of the resonance features. This results in the appearance of doublets for each J-state selection as a consequence of the selection rule $\Delta J=\pm1$ for the one-photon interaction in the B-X system of I_2. For each of the four $\omega_1\approx\omega_{n0}$ resonances listed, the four-photon cycle involves a P and an R transition in the second step. An example of such a doublet is the pair of lines assigned in Fig. 5 as $[P,R,^2S]103$ and $[P,P,^2Q]103$. Resonance enhancement through a continuum can be accomplished for any J state at each frequency position probed. Therefore, no extra selectivity is added to the overall process by resonance enhancement in the continuum. All spectral features in Fig. 5, except for one line marked with an asterisk, are assigned as four-wave cycles with the first interaction corresponding to one of the resonance absorptions listed in Table I. Four initial states are probed, each one giving rise to a doublet. This explains the occurrence of eight pronounced lines in each group of this Raman overtone sequence.

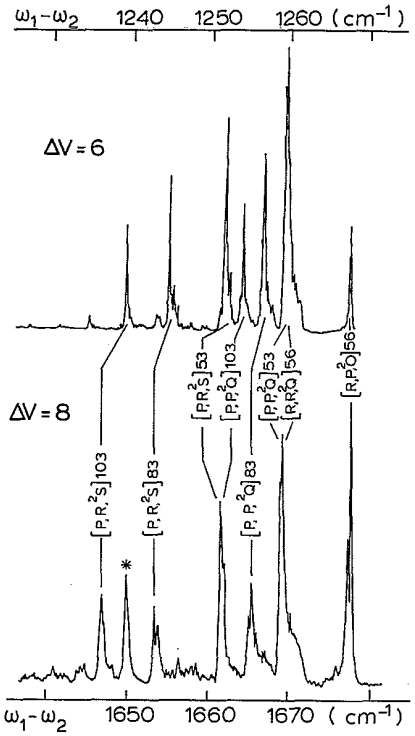

FIG. 5. Observed resonance-enhanced ground-state CARS spectra for $\Delta v=6$ and $\Delta v=8$ Raman overtones with the calculated four-photon cycles. The line marked with an asterisk could not be identified.

As the different overtone Raman transitions share the same electronic enhancement ($\omega_1\approx\omega_{n0}$), the overall structure of these transitions is expected to be identical. Small differences are due to the fact that the rotational constants of different vibrational levels vary because of centrifugal distortion. In Fig. 5 vertical bars between the spectral features in the $\Delta v=6$ and 8 Raman groups connect lines with identical rotational assignments. The FWM features in the $\Delta v=6$ and 8 spectra are found at the calculated positions and are identified by the transition sequences included in Fig. 5.

B. Triply resonance-enhanced CARS

The Raman overtone sequence of the process discussed in Sec. IV A extends into the region of Raman shifts ($\omega_1-\omega_2$) below 1200 cm^{-1} with an uninterrupted regularity in the frequency spacing between the groups ($\sim$200 cm^{-1}). In the sequence $\Delta v=13$-6 only gradual changes in the spectral features within a group were observed. A qualitative change appears, however, in the spectrum at $\Delta v=5$ [see Fig. 6(a)]. Two strong and broadened spectral lines, with an intensity more than an order of magnitude larger than peaks in the $\Delta v=6$ spectrum, dominate the $\Delta v=5$ group. Some minor additional features, related to the double discrete resonance processes in Figs. 3(a)–3(c), are visible as well.

The additional enhancement is a consequence of the fact that the anti-Stokes electronic enhancement is no longer due to the dissociative continuum of the $B\,^3\Pi_{u0}^+$ state. Given the fixed frequency $\omega_1=18\,788.3$ cm^{-1} the energy level probed by the third photon interaction for the $\Delta v=5$ overtone lies well below the dissociation limit $D_e(B)=20\,043.063\pm0.020$ cm^{-1} [29]. In this case the level $|n'''\rangle$ of Eq. 2(a) is a bound state, and the wave-mixing scheme is represented by scheme (d) of Fig. 3. All four transitions coincide with molecular resonances in the $B\,^3\Pi_{u0}^+$–$X\,^1\Sigma_g^+$ band system and the enhancement in this FWM process is called triply discrete in the following. The two broad spectral lines of high intensity in Fig. 6(a) were found to be examples of such triple resonances on discrete levels. From the observed frequency positions both triple resonances could be identified in terms of sequences of four one-photon interactions as listed in Table II. The notation for the lines of this process, included in Fig. 6, correspond to four consecutive P or R one-photon interactions with a specific initial J state.

The intensity observed for the components of the $\Delta v=5$ triple resonance in pure I_2 at 0.3 Torr was found to be comparable to the CARS signal observed for the Q branch of N_2 in air. At each resonance peak the signal in

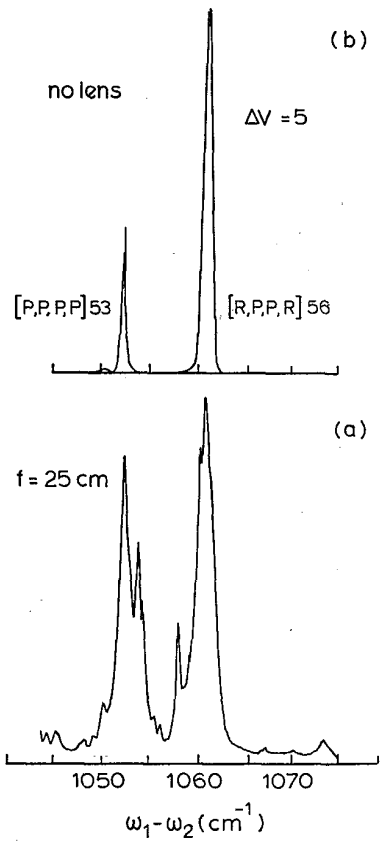

FIG. 6. Observed $\Delta v = 5$ triple resonances with four-photon cycles. (a) Geometry with collinear focused laser beams ($f = 25$ cm lens); (b) without lens.

I_2 is produced by the fraction of molecules in the initial state of the FWM cycle with a particle density of about $N = 7 \times 10^{13}$ cm^{-3}. For comparison, the particle density of a specific quantum state in N_2 in air is 2×10^{18} cm^{-3}.

In an experimental setup in which the focusing lens was left out, the two triple resonances remain of comparable intensity, while other features (originating from double discrete resonances) disappear [see Fig. 6(b)]. An explanation of this effect lies in the fact that the three single one-photon bound-state transitions already saturate at low laser intensities. Enlargement of the interaction volume then gives rise to increased signal for the triple resonances. The intensity of the continuum resonances in FWM, however, depends quadratically on the incident power at ω_1 and is therefore favored in the focusing setup.

Finding a triple resonance in a two-color experiment is a coincidence, even more so in the present investigation where one of the frequencies (ω_1) was kept fixed. The energy-level density in the heavy I_2 molecule is so high that triple resonances were observed not only at $\Delta v = 5$, but also at $\Delta v = 2$, 3, and 4. In Fig. 7 a spectrum of the $\Delta v = 4$ threefold resonant FWM process is shown. The assigned triple resonances are not all precisely resonant with transitions in the $B\,^3\Pi_{u0}^+ - X\,^1\Sigma_g^+$ system. Assuming equal detunings $\delta\omega_2 = \omega_1 - \omega_2 - \omega_{v0}$ and $\delta\omega_3 = \omega_3 - \omega_{n'''0}$ the frequency positions of the observed spectral lines as listed in Table II were calculated. The spectral features of the $\Delta v = 4$ group, as well as of the $\Delta v = 2$ and 3 groups in near triple resonances, are not exclusively related to one of the four absorption resonances listed in Table I. In these spectra features related to initial states with $v = 0$ and $J = 52$, 54, 84, 86, and 87 were observed as well.

The vibrational energy structure in the $B\,^3\Pi_{u0}^+$ and $X\,^1\Sigma_g^+$ states is such that the resonance conditions for the quasi-triple-resonance group $\Delta v = 4$ are not as favorable as for the $\Delta v = 5$ group (see Table II). The three detunings $\delta\omega_1$, $\delta\omega_2$, and $\delta\omega_3$ for the $\Delta v = 4$ case are larger for the resonances assigned. Therefore, the resonance enhancement on the $\Delta v = 4$ feature is expected to be weaker as was indeed the case. Only the strongest features could be assigned unambiguously with a sequence of four transitions and an initial J state (see Table II). The weaker resonances in the energy range of this $\Delta v = 4$ group correspond to quasi-triple-resonances with a set of larger detunings $\delta\omega_i$.

Intensities in the spectra of $\Delta v = 4$ and 5 (Figs. 7 and 6,

TABLE II. Observed triply discrete resonances assigned to $B\,^3\Pi_{u0}^+ - X\,^1\Sigma_g^+(v',v'')$ transitions and the detunings $\delta\omega_1$, $\delta\omega_2$, and $\delta\omega_3$ (in cm^{-1}) of the three resonances. In the last column the frequency positions of the observed spectral lines are given (in cm^{-1}).

Raman overtone	Assignment	$\delta\omega_1$	$\delta\omega_2$	$\delta\omega_3$	$\omega_1 - \omega_2$
$\Delta v = 5$	$[P(32,0),P(32,5),P(60,5),P(60,0)]53$	−0.2	−0.3	−0.3	1052.8
	$[R(32,0),P(32,5),P(61,5),R(61,0)]56$	−0.0	0.2	0.2	1060.6
$\Delta v = 4$	$[P(32,0),P(32,4),R(50,4),R(50,0)]52$	−1.8	−0.3	−0.3	844.8
	$[P(32,0),P(32,4),R(50,4),R(50,0)]53$	−0.2	0.8	0.8	843.7
	$[P(33,0),R(33,4),R(55,4),P(55,0)]87$	3.7	−0.2	−0.2	855.4
	$[P(32,0),R(32,4),R(50,4),P(50,0)]54$	1.5	−0.3	−0.3	836.9
	$[P(33,0),P(33,4),P(54,4),P(54,0)]84$	3.1	−0.4	−0.4	842.9
	$[R(33,0),R(33,4),P(54,4)P(54,0)]84$	−4.2	−0.4	−0.4	842.9
$\Delta v = 3$	$[P(32,0),P(32,3),R(44,3),R(44,0)]53$	−0.2	−0.1	−0.1	635.3
	$[P(32,0),R(32,3),R(44,3),P(44,0)]54$	1.5	−1.0	−1.0	628.3
$\Delta v = 2$	$[P(33,0),P(33,2),P(41,2),P(41,0)]83$	0.5	−1.2	−1.2	424.9
	$[R(33,0),R(33,2),R(41,2),R(41,0)]86$	1.0	0.2	0.2	423.5

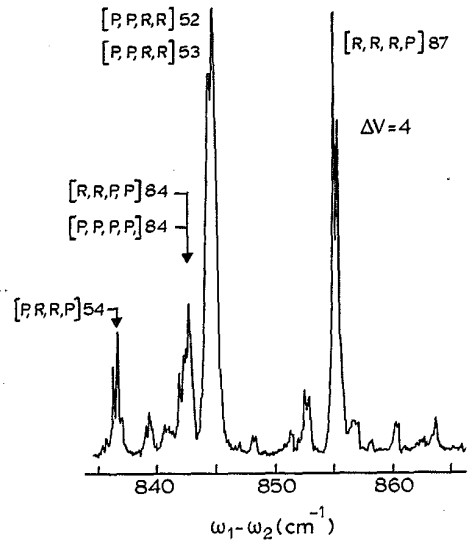

FIG. 7. Observed $\Delta v = 4$ triple resonances assigned to the indicated four-photon cycles.

respectively) are about one order of magnitude larger than those observed in the $\Delta v = 6$ spectra that are related to the resonance-enhanced CARS process with enhancement by two discrete states and one continuum. Theoretically, the difference in line intensity between these processes is mainly due to the different value of the third damping parameter $\Gamma_{n'''0}$, where the state $|n'''\rangle$ is either a bound or a continuum state. The intensity of the FWM signal in the case of the triple resonance is proportional to $|(i\Gamma_d + \delta\omega_d)|^{-6}$ and in all other cases proportional to $\Gamma_d^{-2}|(i\Gamma_{d'} + \delta\omega_{d'})|^{-2}\Gamma_c^{-2}$. Here Γ_d is the relaxation parameter between two bound states (estimated to be <0.01 cm^{-1} even in the case of large collision broadening), Γ_c is the relaxation parameter between a bound state and a continuum, and $\delta\omega_d$ is the detuning parameter on a discrete resonance. The triple resonance signal in the $\Delta v = 5$ spectrum is expected to be roughly 500 times stronger than the signal of the other processes because the detuning of 0.2 cm^{-1} has to be compared with the continuum relaxation parameter, which is estimated to be 5 cm^{-1}. However, because of the small detuning $\delta\omega_3$ in this case of the triple discrete resonance, there is a stronger absorption of the ω_3 anti-Stokes wave. Saturation of the triple discrete resonance hampers a quantitative comparison. Saturation aspects are outside the scope of the present perturbative approach of multiresonance features.

C. Excited-state parametric CARS

The observed spectrum for Raman shifts $\omega_1 - \omega_2 = 850 \rightarrow 1160$ cm^{-1}, partly depicted in Fig. 8, shows groups of repeating structures with a frequency separation of about 25 cm^{-1}. This spectrum may be explained assuming Raman resonances in the vibrational levels $v' = 50$–60 of the $B\,^3\Pi_{u0}^+$ excited state [scheme (f) in Fig. 3], thus with $(\omega_1 - \omega_2) \approx \omega_{n''n}$. A Raman shift of about 900 cm^{-1} corresponds to an energy difference between $B\,^3\Pi_{u0}^+$ $v' = 32$ and 52 levels. The observed resonances can be assigned with four consecutive photon interactions as indicated in Fig. 8.

In the four-wave cycle of this process the interaction of the first photon is again the state-selective step by the resonance $\omega_1 \approx \omega_{n0}$. Lines involving $P(53)$ and $R(56)$ transitions of the B-$X(32,0)$ band in I_2 are again the main features as in the resonance-enhanced CARS. By tuning ω_2 a coherence between states $|n\rangle$ and $|n''\rangle$ is established by the second and third photon of frequencies ω_1 and ω_2, respectively. This Raman resonance for a selected J state is enhanced by the continuum in a Q branch and in an S or O branch. Only one of the latter two is allowed for the completion of the four-photon $\Delta J = 0$ cycle. In all cases the FWM cycle is completed by a resonance P or R emission. The anti-Stokes wave is electronically enhanced by $\omega_3 = \omega_{n''0}$. Thus, for each of the selected $R(56)$ and $P(53)$ transitions two pathways in the FWM cycle exist, and doublets of the initially probed levels appear again in the spectrum. Some of the weaker features in the spectrum can be accounted for by the four-photon cycles involving the $P(83)$ one-photon resonances ω_{n0}.

As mentioned in Sec. II A the energy-level diagrams of scheme (f) and scheme (b) of Fig. 3 show identical discrete resonances for the (ω_1) and $(2\omega_1 - \omega_2)$ interactions. Both processes contribute to lines at the same frequency positions $(\omega_1 - \omega_2)$ and are identical as far as line positions are concerned. If the spectral features of Fig. 8 are interpreted in terms of scheme (b), the detunings $\delta\omega_2 = \omega_1 - \omega_2 - \omega_{v0}$ for each particular resonance can be calculated. The smallest detunings obtained for the most pronounced spectral lines, i.e., for the overtone sequence $[R, {}^2Q, R(v')]56$ for $v' = 52$, 53, and 54, are $\delta\omega_2 = 38$, 63, and 86 cm^{-1}, respectively. For the second strongest vibrational sequence $[P, {}^2Q, P]53$ the detunings are $\delta\omega_2 = 50$, 75, and 99 cm^{-1}.

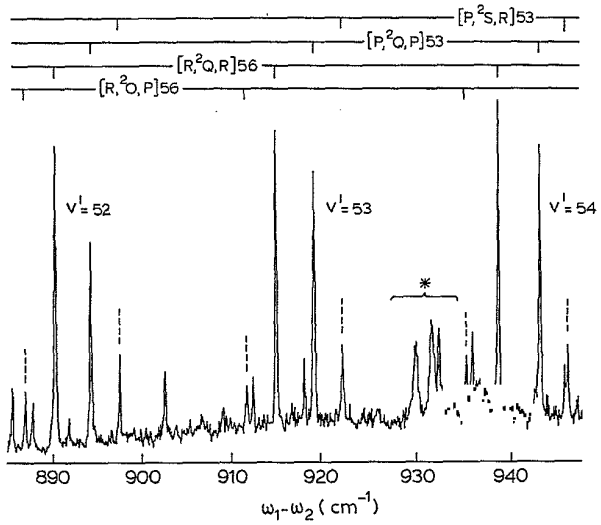

FIG. 8. Observed four-wave-mixing features of the excited-state parametric CARS process in I_2. The lines marked with an asterisk correspond to the $v' = 20$ resonances of the excited-state nonparametric process of scheme (g) in Fig. 3.

The observed intensity distribution over the Raman overtone sequence in Fig. 8 varies smoothly. Furthermore, the observed relative intensities between doublets, such as $[R,{}^2Q,R]56$ and $[R,{}^2O,P]56$, are constant in this region. In the case of scheme (f) being the dominant contributor to the excited-state parametric CARS process, indeed a smooth intensity dependence with respect to vibration is expected. The vibrational overlap function between the discrete $B\,{}^3\Pi_{u0}^+|v\rangle$ states and the repulsive continuum $|c\rangle$ will vary only slightly for adjacent $|v\rangle$ levels. In the case of scheme *b* as the dominant contributor to the observed lines in Fig. 8, one would expect an intensity drop of a factor of 5 for the strongest $J=56$ lines when going from $v'=52$ to 54. The intensity is namely proportional to $(1/\delta\omega_2)^2$. However, a smooth and regular intensity variation for the adjacent overtones is observed. It is this argument which proves that scheme (f) is the dominant one. So, we conclude that the excited-state parametric CARS process is enhanced by the repulsive continuum $|c\rangle$ at the two-photon level.

However, on following this sequence up to higher vibrational states v', scheme (b) will become important as the detuning from resonance decreases. At $v'=60$ and 61 scheme (b) even coincides with the triply resonance-enhanced CARS process of scheme (d). And in fact the triple resonances observed in Fig. 6 involve $v'=60$ and 61 (see also Table II).

D. Excited-state nonparametric CARS

A third sequence of repeating groups of several resolved lines was observed in the range $\omega_1-\omega_2=850$–2200 cm^{-1}. The similarity in appearance of these groups suggests again an energy scheme with at least one selective, discrete resonantly enhanced interaction. The frequency separation of about 100 cm^{-1} between these repetitive structures, slowly decreasing with a smaller value of the Raman shift $\omega_1-\omega_2$, indicates another Raman overtone sequence in the $B\,{}^3\Pi_{u0}^+$ state near $v'=15$. The features shown in Fig. 9 could be unambiguously assigned with the four-photon scheme (g) of Fig. 3. This is a nonparametric FWM process as given by the double-Feynman diagrams III in Fig. 2. This process was not proposed and/or observed before in resonance-enhanced FWM studies in I_2. A group of lines corresponding to this process also appears in Fig. 8. The calculated line positions coincide accurately, within the experimental error, with the Raman shift $\omega_1-\omega_2\approx\omega_{nn'}$. The $J=103$ state is not resonant with the $v'=13$ and 16, but with the $v'=14$ and 17 levels, respectively, and it is mere coincidence that it appears so close to the other repetitive lines. The resonances originating from the $J=83$ level appear in a different energy region and are not present in the spectra shown in Fig. 9.

In this process a pair of photons (ω_1,ω_2) creates a coherent superposition of states $|n\rangle$ and $|n'\rangle$, both rovibrational levels of the $B\,{}^3\Pi_{u0}^+$ state. This coherence is only produced effectively when both ω_1 and ω_2 are in electronic resonance with the *B-X* system and share an initially populated state $\rho_{00}^{(0)}$. As the Stokes frequency ω_2 is tuned the superposition is created for those states for

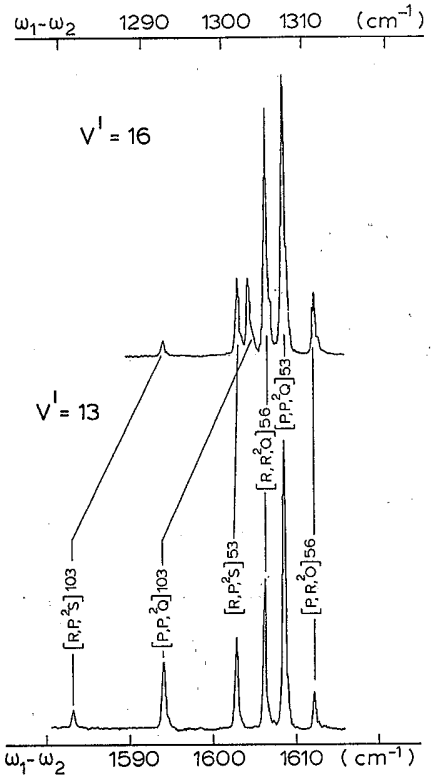

FIG. 9. Observed features of the excited-state nonparametric four-wave-mixing process of scheme (g) in Fig. 3.

which the resonance condition $\omega_1\approx\omega_{n0}$ holds. It must be stressed again that the *coincidental* resonance enhancement through the fixed ω_1 photon is the same as in all other processes. For each selected initial state (of Table I) the coherent superposition of $|n\rangle$ and $|n'\rangle$ can be created either by a *P* or *R* transition in resonance with ω_2. Therefore tuning of ω_2 again results in doublets in the spectra. The four-photon cycles are then completed by either a *Q* and *O* or a *Q* and *S* two-photon continuum-enhanced resonance. The full four-photon cycle in this process does not obey the $\Delta J=0$ rule as the initial and final states differ in a one-photon transition in which population is transferred to an electronically excited state.

Again it should be noted (as in Sec. II A) that the resonances of scheme (g) also appear in scheme (h). Scheme (h) in principle contributes to FWM resonances identified here as related to scheme (g), and on the grounds of line positions only these contributions cannot be ruled out. However, detunings $\delta\omega_{\rm det}=\omega_1-\omega_2$ in the case of scheme (h) are as large as 2200 cm^{-1}. The damping parameter related to enhancement by the continuum $|c\rangle$ was estimated (Sec. II A) to be smaller than 50 cm^{-1}. Considering the quadratic dependence of the intensity on either the inverse detuning [in the case of scheme (h)] or the inverse damping [in the case of scheme (g)] we conclude that it may be considered unlikely that scheme (h) has any significant contribution to the excited-state nonparametric CARS process. In addition we note here that

the absolute intensity of this nonparametric CARS process is of the same order of magnitude as the resonance-enhanced ground-state CARS process for which continuum enhancement undoubtedly plays a role.

V. SUMMARY

In conclusion, all intense features observed in the range $\omega_1-\omega_2=380-2300$ cm^{-1}, where a frequency $\omega_3=2\omega_1-\omega_2$ is produced, could be assigned as spectral components of one of three different Raman FWM processes. Apart from some additional irregular weak lines, probably far off-resonance features, the observed lines were identified and found to coincide with calculated positions. In a theoretical paper by Druet *et al.* [4] the importance of doublets in resonance CARS was stressed as being a tool for the assignment of lines. The spectra shown in Figs. 5, 8, and 9 indeed contain doublets corresponding to a common initial J state. However, a cursory inspection of the spectra does not simply lead to an identification of the partners within such a doublet. For a correct assignment it is necessary to follow the procedure of calculating the sequence of photon resonances.

A few general remarks can be made concerning the relative intensities between sequences of overtone groups for each process. The relative intensities of the different overtones vary slightly, except in the case of the triple discrete resonance, due to the slowly varying Franck-Condon factors [30] and the vibrational dependence of continuum enhancement. As the overtones appear in a wide frequency range ($\omega_1-\omega_2$), where dye yield and transmission of interference filters may vary considerably and experimental conditions (power density and overlap of the beams in the focus) cannot be kept constant, only relative line intensities within the small-wavelength interval of a single resonance group can be considered.

Within each resonance group the relative intensity of the spectral lines is determined by a product of (near-) resonance denominators, the oscillator strengths of four consecutive photon interactions and the population density of the initial state probed. A detuning $\delta\omega_1=\omega_1-\omega_{n0}$ of the fixed frequency ω_1 in one of the denominators (listed in Table I) is common to all processes. Stronger lines are expected in the case of FWM features involving e.g., $P(53)$ or $R(56)$ transitions compared to lines involving $P(83)$, where the detuning is larger. In all observed spectra, most easily seen for the excited-state CARS processes in Fig. 8 and in Fig. 9, the FWM sequences involving $P(53)$ and $R(56)$ transitions are indeed the stronger ones.

As far as *linewidths* and *line shapes* of FWM resonances are concerned, the spectral features of the Raman resonances in the electronic excited state appear as single, resolved lines with a width equal to the bandwidth of the tunable laser $\Delta\omega_c=0.3$ cm^{-1}. The resonance enhanced CARS spectra shown in Fig. 5 and corresponding to scheme (e) in Fig. 3, show line broadening in the form of asymmetries that are due to unresolved substructure. The triple discrete resonances clearly show effects of power broadening, even in the setup with unfocused laser beams [Fig. 6(b)].

VI. CONCLUSION

In the present paper the experimental observation of a number of multiresonance CARS processes is reported, some of which were predicted in theoretical papers by Oudar and Shen [9] and by Druet and Taran [7]. In the gaseous medium molecular iodine, essentially three different sequences of multiresonance features were observed which can be viewed as three different coherent Raman overtone series; one in the ground electronic state, and two in an electronically excited state. The line positions of the FWM features could be explained precisely on the basis of the accurately known spectroscopic constants of the B-X system in I_2. The relative intensities of the spectral lines observed in the different overtone series are not accounted for in the present study. For an explanation of intensities, the product of four transition dipole moments in a coherent four-photon process needs to be calculated. In a forthcoming paper [16] these aspects and also the implications of arbitrary polarizations of the field vectors will be described. Moreover, the asymmetric line shapes, as observed in particular in the resonance-enhanced ground-state CARS process, are currently being studied using pulsed lasers with smaller bandwidths. A preliminary result is that the asymmetries are not produced by saturation broadening.

The lines in the FWM spectra of the three processes, resonantly enhanced by two discrete states and one continuum, were of comparable overall intensity but weaker than the triply discrete resonances discussed in Sec. IV B. All single resonance features in the FWM spectra probed population of states which were selected by the absorption resonance of the wave at ω_1. For the present choice of the frequency-doubled Nd:YAG laser at 18 788.3 cm^{-1} a quartet of rotational states in the $X\,^1\Sigma_g^+, v=0$ ground state of I_2 was selected: $J=53$, 56, 83, and 103. The ground-state CARS process was shown to be resonantly enhanced by predominantly the $B\,^3\Pi_{u0}^+$ continuum at the one-photon level. In this paper arguments are presented that illustrate the enhancement in the excited-state CARS processes at the two-photon level by a continuum state, supposedly of 0_g^+ character, with maximum absorptivity at an energy of 37 700 cm^{-1} above the ground state [25,26].

In the theoretical section a generalized energy-level structure consisting of two bound electronic states and a continuum at the two-photon level was postulated. This system was shown to be appropriate in the case of I_2, as the three observed Raman overtone series could be explained using the appropriate interpretation of $\chi^{(3)}$ in terms of this general energy scheme.

Of practical importance is the fact that a very strong triple resonance can be induced in I_2 with the fixed-frequency-doubled photons from a Nd:YAG pump in a two-color setup, even without making use of a focusing lens. This result bears promise for a possible use of triply discrete resonance-enhanced CARS as a detector for radioactive iodine fission products, most notably $^{131}I_2$ *in situ* in an operating nuclear factor. For this purpose collisonal quenching effects on the signal intensities of triple resonances are planned to be studied in the near future.

ACKNOWLEDGMENTS

The authors are grateful to B. Attal-Trétout and J.-P. Taran (ONERA, Paris) for their stimulating interest in our experiments, for reading a first draft of the manuscript and for valuable comments. We also thank M. Müller (University of Amsterdam) for his help in the derivation of the appropriate double-Feynman diagrams. This work was supported in part by KEMA (Arnhem, The Netherlands).

[1] S. Gerstenkorn and P. Luc, *Atlas du Spectre d'Absorption de la Molécule d'Iode* (Editions du CNRS, Paris, 1977).
[2] D. L. Rousseau and P. F. Williams, J. Chem. Phys. **64**, 3519 (1976).
[3] N. Bloembergen, H. Lotem, and R. T. Lynch, Ind. J. Pure Appl. Phys. **16**, 151 (1978).
[4] S. A. J. Druet, B. Attal, T. K. Gustafson, and J.-P. Taran, Phys. Rev. A **18**, 1520 (1978).
[5] S. Y. Yee, T. K. Gustafson, S. A. J. Druet, and J.-P. Taran, Opt. Commun. **23**, 1 (1977).
[6] Y. Prior, IEEE J. Quantum Electron. **QE-20**, 37 (1984).
[7] S. A. J. Druet and J.-P. Taran, Prog. Quantum Electron. **7**, 1 (1981).
[8] S. A. J. Druet, J.-P. Taran, and C. Borde, J. Phys. (Paris) **40**, 819 (1979).
[9] J.-L. Oudar and Y. R. Shen, Phys. Rev. A **22**, 1141 (1980).
[10] S. Mukamel and R. F. Loring, J. Opt. Soc. Am. B **3**, 595 (1986).
[11] Y. Prior, A. R. Bogdan, M. Dagenais, and N. Bloembergen, Phys. Rev. Lett. **46**, 111 (1981).
[12] A. Beckman, H. Fietz, P. Baierl, and W. Kiefer, Chem. Phys. Lett. **86**, 140 (1982).
[13] B. Attal, O. O. Schnepp, and J.-P. Taran, Opt. Commun. **24**, 77 (1978).
[14] S. S. Dimov, L. I. Pavlov, K. V. Stamenov, and K. V. Khadzhiisky, J. Raman Spectrosc. **17**, 277 (1986).
[15] P. Luc, J. Mol. Spectrosc. **80**, 41 (1980).
[16] I. Aben, W. Ubachs, G. van der Zwan, and W. Hogervorst (unpublished).
[17] E. Yarkoni and Y. Prior, IEEE J. Quantum. Electron. **QE-20**, 43 (1984).
[18] G. Fujimoto and T. K. Yee, IEEE J. Quantum. Electron. **QE-19**, 861 (1983).
[19] G. Herzberg, *Molecular Spectra and Molecular Structure, Vol. I: Spectra of Diatomic Molecules* (Van Nostrand, New York, 1950).
[20] K. K. Lehmann, J. Smolarek, and L. Goodman, J. Chem. Phys. **69**, 1569 (1978).
[21] M. S. De Vries, N. J. A. van Veen, and A. E. De Vries, Chem. Phys. **56**, 157 (1981).
[22] C. Tai, F. W. Dalby, and Gordon, L. Giles, Phys. Rev. A **20**, 233 (1979).
[23] J. C. D. Brand and A. R. Hoy, Appl. Spectrosc. Rev. **23**, 285 (1987).
[24] G. W. King and T. D. McLean, Mol. Spectrosc. **135**, 207 (1989).
[25] R. K. Sander and K. R. Wilson, J. Chem. Phys. **63**, 4242 (1975).
[26] G. E. Busch, R. T. Mahoney, and K. R. Wilson, J. Chem. Phys. **51**, 837 (1969).
[27] K. Kasatani, Y. Tanaka, K. Shibuga, M. Kawasaki, K. Obi, H. Sato, and I. Tanaka, J. Chem. Phys. **74**, 895 (1981).
[28] P. Baierl and W. Kiefer, J. Raman Spectrosc. **11**, 393 (1981).
[29] M. D. Danyluk and G. W. King, Chem. Phys. **25**, 343 (1977).
[30] J. Tellinghuisen, J. Quant. Spectrosc. Radiat. Transfer **19**, 149 (1978).
[31] J. W. Nibler and J. J. Yang, Annu. Rev. Phys. Chem. **38**, 349 (1987).